Invention Journal of Research Technology in Engineering & Management (IJRTEM)
ISSN: 2455-3689
www.Ijrtem. com Volume 3 Issue 6 ǁ September-October 2019 ǁ PP 16-26

Evaluation of Williamson–Hall strain and Electrical properties in WO3@NaDCC/ITO nanoparticles thin films prepared by Hydrothermal method

[1,]Mohanad Q. Kareem, [2,]Nadim K. Hassan
[1]*Department of Physics, College of Science, University of Kirkuk, Kirkuk, Iraq*
[2]*Department of Physics, College of Education, University of Tikrit, Tikrit, Iraq*

ABSTRACT : *Herein , we report the firstly, hydrothermal technique at temperature 200°C with annealing temperature at 600°C (for I hour) to depositions tungsten oxide thin films with different doping concentrations of Sodium dichloroisocyanurate NaDCC (0,2 and 4)wt% on ITO substrates with thicknesses about 100 nm , characterized with Field Emission scanning electron microscope (FESEM), electron dispersive spectroscopy (EDS) , X-ray diffraction (XRD), , hall effect measurement , direct currents and analysis to study the structural, morphological and electrical properties. The elemental composition of that nanocomposite thin films (W, O and In) determined from EDS. An X-ray diffractions pattern confirmed the formation of polycrystalline monoclinic structure for WO3/ITO and WO3@NaDCC, ITO has a cubic in structure. The Williamson–Hall plot drawn for evaluating the micro-strain and crystallite diameter. Morphology analyzed by field emission scanning electron microscopy (FESEM). The results expressed the formation of nanoparticles. In addition on it, The mechanisms of dc conductivity of un-doped WO3/ITO and doped withWO3@ NaDCC (2 and 4)wt.% /ITO thin films on at the range (303 to 473) K have discussed ,there is a decrease in conductivity with the increase in the doping concentration, and hall measurements show that all films have a negative hall coefficient and carrier concentration (n) increases with the rise of doping ratio and decreasing in carrier mobility (μ_H) with swelling of NaDCC .*

KEYWORD : *Tungstenoxide; Hydrothermal Technique; NaDCC; morphology; Williamson-Hall; electrical properties.*

I. INTRODUCTION

In the last decade, nanomaterials play a crucial role in different fields of science like biology, medicine, pharmacology, and water industry, marking a positive attitude toward this research field more than over [1]. Researchers in the electrical engineering fields, chemistry, and physics are focusing on the interest in the development and characterization of nanocomposite materials[2]. Preparation of metal -oxide, and transition metal doped semiconductor nanomaterials supply opportunities for improving the application in different areas of science and technology because of their individual chemical and physical properties caused by their nano-sized dimensions and large surface/volume ratio [3].The production of nanostructures with a phase-controlled procedure is still an affront for material scientists, and there is a great advantage in developing new methods to adopt phase-controlled synthesis. Recently, tungsten oxide and its compounds are focusing because of their unusual physical and chemical properties in the nanoscale regime. Tungsten trioxide (WO_3) is Avery promising metal oxide with varying properties .it has an n-type (Eg=2.6 –3.75) eV semiconducting nature and unique electrical properties [4]. It has been used in many fields due to its cost-effective, simplicity, self-cleaning [5], and environmental friendly and low toxicity such as gas sensor , field emission devices , solar energy devices and smart windows [6], [7] ,high- efficiency photocatalysis [8] , metal secondary battery[9] , full cell and photochemical water splitting [10] .

Tungsten trioxide in a thin -film structure is more desirable for various device applications because thin solid films can be integrated into small devices or combined with other materials to form composites for scientific applications.WO_3 is a promising photocatalyst due to its non-toxic nature, having high phot,o-corrosion resistance and physicochemical stability [11].A variety of techniques have developed to control the structure and morphology of WO_3 material like sputtering, thermal evaporation, template synthesis, chemical synthesis, and hydrothermal method. Among them, hydrothermal is becoming a more preferred method of synthesis WO_3. This process requires relatively low power and non-sophisticated equipment which is a suitable route to achieve mass and economies of scale production system requirement [12]. This study reports the effect of sodium-dichloroisocyanurate (NaDCC) as “reservoir chlorine” because of chemical equilibrium as a strong directing agent in producing dagger-like moonflowers or nanoparticles … etc. via a facile hydrothermal process [13], [14].

In this research the essential aim of work to prepare a pure WO3 on ITO thin films and doped with NaDCC by using Hydrothermal method at 200ºC at different concentration (0, 2, and 4) %wt/ITO. and study the structural and electrical properties of these prepared samples.

II. MATERIAL AND METHODS

Preparation :WO3 porous structures synthesized by the hydrothermal method. In a typical, the usually prepared solution prepared by dissolving 1.65 g of ammonium para tungstate dehydrate in 20 mL distilled water under magnetic stirring for 10 min to get a clear answer. The pH of this solution was (8). Subsequently added (2,4) wt% of Sodium dichloroisocyanurate (NaDCC) and several drops of HCl were introduced to attain the pH value of 1. Here the adding HCl can act as a precipitating agent and also medium for the product to have desired morphology, a transparent yellow solution with foam obtained, and These solutions transferred into a 100 mL Teflon-lined stainless steel autoclave with filling about 50% of the whole volume by added distilled water. ITO substrate was dipped vertically in the autoclave, maintained at 200 c for 6h and then cooled down to room temperature. The WO3@NaDCC/ITO thin films were rinsed with distilled water and ethanol for three times to neutralize the pH of the solution respectively, the surrounding water present in the product was removed by the drying process at 60 C in air for 1 hr. To observe the effect of Sodium dichloroisocyanurate (NaDCC), The process was repeated in the absence of Sodium dichloroisocyanurate (NaDCC) under identical conditions. Finally, the thin films were annealed at deferent temperatures 600 Co in the oven for one h for investigating the crystal structure, morphology, and optical properties. The final product without the assistance of NaDCC was named as WO3/ITO while that with the support of NaDCC was named as WO3@NaDCC/ITO.

Characterization Details : The X-ray diffraction line profile data are recorded in a continuous scan mode (2θ = 10-80) using X'Pert PRO (PAN analytical) diffractometer in the Bragg–Brentano par focusing configuration ($\theta/2\theta$ geometry) with CuKα (λ = 1.5406 A˚) radiation at room temperature (25 C). The electrons, emitted from the cathode filament accelerated towards the anode plate (Cu) by applying 40 kV voltage and 30 mA filament current. An X-ray diffractometer, the diffraction beam optics equipped with 0.04 rad solar slit, fixed divergent slit (slit size = 0.8709), 0.100 mm size receive slit and a scintillator detector. The samples are scanned with a constant step of 0.05 deg of 2θ and with constants counting time of 1.5sec at each level to minimize the instrumental contribution in XRD line broadening. Particle size and morphology were examined under vacuum by the field emission scanning electron microscopy (FESEM). Fitted with Energy-dispersive X-ray spectroscopy (EDAX) [Model: FE-SEM. TESCAN MIRA3/RAITH LIS. France], with ITO glass acting as a blank. Aluminum electrodes by using a suitable mask deposited on the surface of the WO3/ITO mixed by thermal evaporation using the Edward coating unit. The connections between the aluminum and very few copper wire made by high conductive silver. A vacuumed closed chamber, by rotary at approximately (1×10^{-2} mbar)was made of stainless steel with a controlled hot plate. A multi-pins feed through at the base of the chamber allows the electrical connections to established to the heater, thermocouple, and sensor electrodes. The sample put on the heater, and the electrical resistance of the sensor measured by the multimeter.

III. RESULTS AND DISCUSSION

Structural studies : Figure 1 shows the XRD pattern for pure WO3 / ITO and WO3@NaDCC /ITO mixed thin films prepared at (2, 4) % wt NaDCC content by hydrothermal method. As seen in Figure 1, all diffraction peaks of WO3 are assigned well to the monoclinic structure of a tenorite system. The major peaks are observed at (2θ = 23.16º, 23.66º, 24.37º, 26.59º, 28.76º, 33.36º, 34.23º, 41.68º, 47.67º, 49.99º, 52.3º , 56.01º) attributed to the (002) , (020) , (200) , (120) , (112) , (022) , (202) , (222) , (004) , (400) , (024) , (142) planes for a monoclinic structure . Showing a single-phase WO3 formation, which is in agreement with JCDS card No: 72-1465. Also, the cubic structure of In2O3, which identical with standard card number JCDS card No: 71-2194). The three patterns show a polycrystalline structure. The pattern for pure sample shows low crystalline, the second and third pattern at (2,4) % wt. NaDCC illustrates increasing in X-ray diffraction peaks intensities, which indicate enhanced the crystalline and a greater number of peaks. The Indium oxide peaks appear to be with less width at half maxima, demonstrating increasing in the crystalline size of the indium oxide at this ratio. Increasing the crystalline size at this ratio may be due to that WO3@NaDCC additive act as catalysis, which enhances the growth of crystals. The broadening of the peaks in X-ray diffraction indicates that the size is in the range of nano size. The grain size of the particulates can be estimated using the Scherer method. It is a most simplified formulation and therefore still employed to estimate the ''apparent'' domain sizes of physical broaden peak profile.

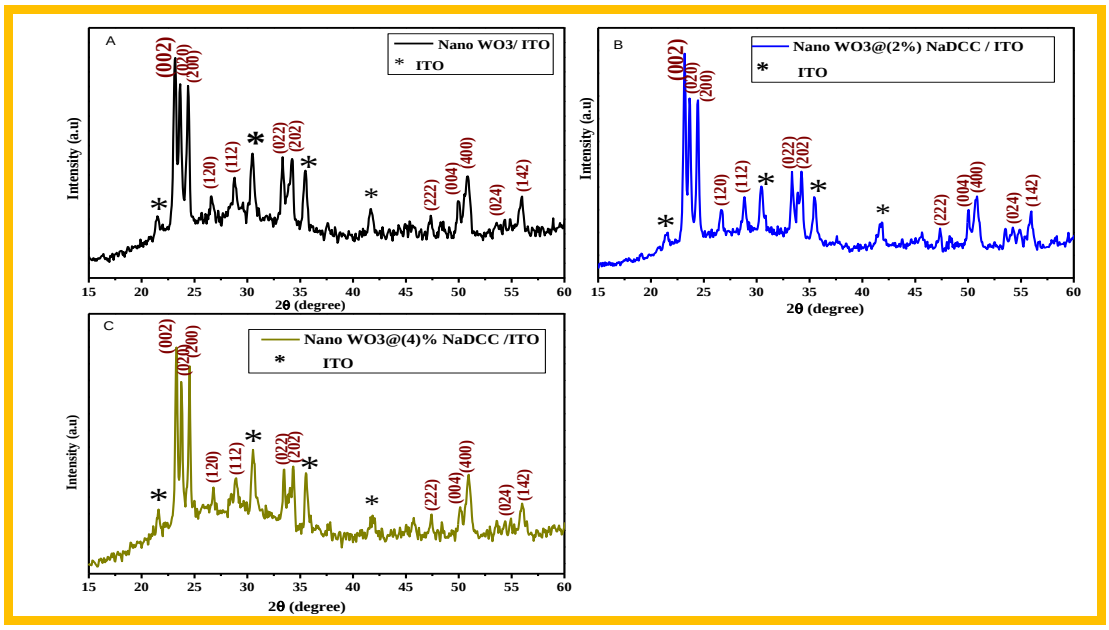

Figure 1. XRD patterns of (A) WO3, (B) WO3@(2%) NaDCC and (C) WO3@(4%) NaDCC nanoparticles deposited onto ITO glass substrates by hydrothermal method and annealing at 600°C.

This method defines the crystallite size in terms of a mean effect size of the coherently scattering region normal to the reflecting planes. The Scherer relation between crystallite size and integral breadth is given by [15]:

$$D = \frac{K\lambda}{\beta D \cos\theta}, \beta_D = \frac{K\lambda}{D \cos\theta} \quad (1)$$

Where D is the adequate crystallite size normal to the reflecting plane, K is a shape factor =0.9), k is the wavelength of CuKα radiation, β_D is the integral width of a particular peak and Θ is the diffraction angle. From Eq. (1), size broadening is independents of the order of a reflection. The dislocation density (δ), defined as the length of dislocation lines per unit volume of the crystal, can be estimated using the following relation:

$$\delta = \frac{1}{D2} \quad (2)$$

The smaller value of dislocation density shows the better crystallization of the film along a particular plane. The observed values of D along different crystallographic planes reported in Table (1,2,3).

Table 1. Structural parameters, interplanar spacing, crystalline size of pure nanoparticles WO3 thin films deposited on ITO glass substrate, annealing T= 600°C.

Sample	2Θ	FWHM (°)	β(rad)	hkl	d_{hkl} (A)	Scherrer method D_{sch} (nm)	δ(nm)$^{-2}$	Av (nm
WO3	23.1642	0.3343	0.005836984	002	3.8367	24.3	0.00167	21.111
	23.6657	0.2925	0.005107143	020	3.7565	27.7	0.00130	
	24.3761	0.2926	0.005108889	200	3.6486	27.8	0.00129	
	26.591	0.5015	0.008756349	120	3.3495	16.3	0.00376	
	28.7642	0.5022	0.008756350	112	3.1012	16.4	0.00371	
	33.3612	0.3344	0.00583873	022	2.6836	24.8	0.00162	
	34.2388	0.4597	0.008026508	202	2.6168	18.1	0.00305	
	41.6776	0.4599	0.008026505	004	2.1653	18.5	0.00292	
	49.994	0.5433	0.00948619	400	1.8229	16.1	0.00385	
	56.0119	0.5431	0.00948622	142	1.6405	16.6	0.00169	

Table 2. Structural parameters, interplanar spacing, crystalline size of pure nanoparticles WO3@ (2%) NaDCC thin films deposited on ITO glass substrate, annealing T= 600^{O}C.

Sample	2Θ	FWHM (°)	β(rad)	hkl	d_{hkl} (A)	Scherrer method D_{sh} (nm)	$\delta(nm)^{-2}$	Av (nm)
WO3 @ (2%) NaDCC	23.2060	0.2090	0.003649206	002	3.8299	38.8	0.00066	24.149
	23.6657	0.2507	0.004377302	020	3.7565	32.4	0.00095	
	24.4597	0.2508	0.004379048	200	3.6363	32.4	0.00097	
	26.7164	0.3761	0.006566825	120	3.3341	21.7	0.00212	
	28.8478	0.5015	0.008756349	112	3.0924	16.4	0.00371	
	33.3612	0.3343	0.005836984	022	2.6836	24.8	0.00162	
	34.2388	0.4597	0.008026508	202	2.6168	18.1	0.00305	
	41.8866	0.5015	0.008756349	004	2.1550	17.0	0.00346	
	49.3612	0.4180	0.007298413	400	1.9179	20.8	0.00231	
	56.0358	0.3344	0.00583873	142	1.8215	26.2	0.00145	

Table 3. Structural parameters, interplanar spacing, crystalline size of pure nanoparticles WO3@ (4%) NaDCC thin films deposited on ITO glass substrate, annealing T= 600^{O}C.

Sample	2Θ	FWHM (°)	β(rad)	hkl	d_{hkl} (A)	Scherrer method D_{sh} (nm)	$\delta(nm)^{-2}$	Av (nm)
WO3 @ (4%) NaDCC	23.2060	0.318653	0.005563789	002	3.8299	24.3	0.00169	24 .777
	23.7493	0.320138	0.005589715	020	3.7435	27.8	0.00129	
	24.5433	0.322371	0.005628714	200	3.6241	32.4	0.00095	
	26.8000	0.328533	0.005736291	120	3.3239	21.7	0.00212	
	28.8896	0.334754	0.005844915	112	3.0880	21.8	0.00210	
	33.4448	0.348058	0.00607721	022	2.6771	28.4	0.00123	
	34.3224	0.350670	0.006122815	202	2.6106	24.9	0.00161	
	41.8448	0.375272	0.006552375	004	2.1571	15.7	0.00405	
	49.4448	0.405369	0.007077886	400	1.8172	21.0	0.00226	
	56.1612	0.419092	0.007317485	142	1.6393	21.5	0.00216	

The strain-induced peak broadening resulting from lattice distortion (macro strains) can expressed by Wilson formula:

$$\varepsilon = \frac{1}{4}\beta_s \cot\theta \ , \beta s = 4\,\varepsilon\, tan\theta \qquad (3)$$

Where ε is the macro strains, and βS is integral breadth due to strain effect. Another method is The Williamson–Hall method is a simple visualization of order dependence peak broadening. In this method, assumed that the size and strain contribution to the line broadening are mutually independent of each other and closely approximated by Cauchy's function and corresponding integral breadths are linearly additive:

$\beta_{hkl} = \beta_D + \beta s$ (4)

Putting the value of βD and βS from Eq. (1) moreover, (3), we get

$$\beta_{hkl} = \frac{K\lambda}{D\cos\theta} + 4\varepsilon \sin\theta \quad (5)$$

By rearranging equation (5)

$$\beta_{hkl}\cos\theta = \frac{K\lambda}{D} + 4\varepsilon \sin\theta \quad (6)$$

After plotting the values of βhkl cosθ as a function of 4sinθ, the intercept on the vertical axis is a measurement of the volume of the domains which diffracted coherently, and the slope gives ‘‘effective’’ strain. Equation (6) represents the uniform deformation model (UDM) of W–H method, in which strain is assumed to be uniform in all crystallographic direction.

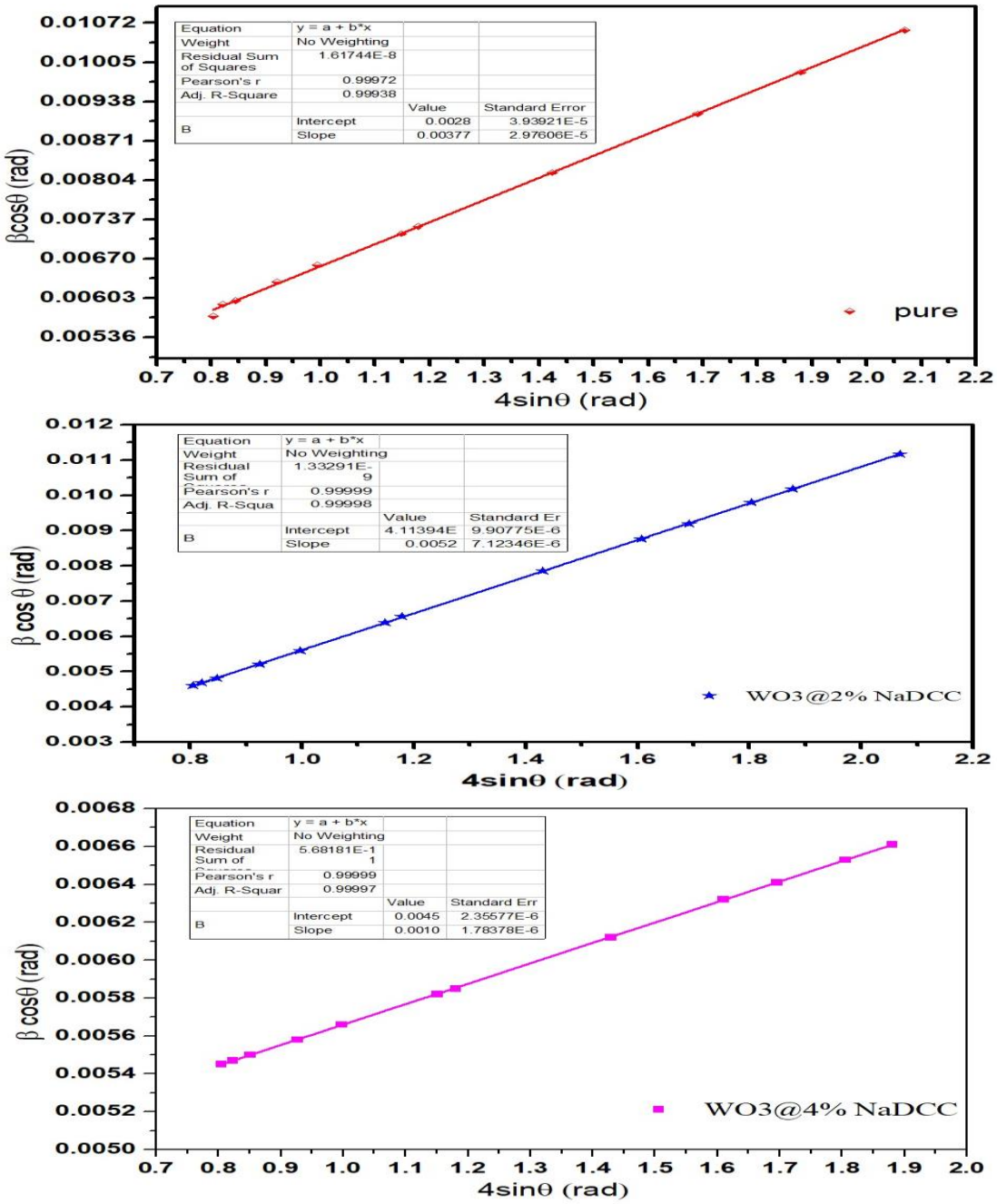

Figure 2. Williamson -Hall plots of the of WO3, WO3@(2%) NaDCC and WO3@(4%) NaDCC nanoparticles deposited onto ITO glass substrates by hydrothermal method and annealing at 600ºC.

Table 4. Geometric parameters of the samples

samples	Scherrer method		Williamson method	
	D_{sh} (nm)	$\delta x10^{-3}(nm)^{-2}$	D_{W-H} (nm)	$\varepsilon x10^{-3}$
WO3	21.11	2.58	27.42	3.77
WO3@(2%)NaDCC	24.15	2.24	32.1	5.21
WO3@(4%)NaDCC	24.77	1.84	27.08	1.09

Thus, the isotropic nature of the crystal considered where material properties are assumed to be independent of the direction along which they measured. This presumption is doubtful, and therefore, in the other variant of the W–H method, a more natural approach is adopted by considering an anisotropic magnitude of strain. The uniform deformation model of WO3@(0, 2, 4) % wt NaDCC / ITO thin films are shown in Fig (2) and Table (4). Respectively.

FESEM compositional analysis : Fig 3 (A) and (B) are the FESEM images of the WO3 thin film on ITO after annealing at 600c. The small round shape-like structure or termed as WO3 nanoparticles can see from the surface morphology of the tungsten oxide films. It is understood the diameter of the formed WO3 is non-uniform size distribution with agglomerates. The average size of approximately ~ 46 nm. These structures were formed throughout the whole surface of the sample, as seen from the inset image in Fig 3 (A). Fig 3(B) shows the cross-sectional view of the oxide with thickness in the range of 70.14 nm to 78.25 nm. Fig 3 (C) shows the EDX analysis of nano WO3/ITO.The EDX analysis was conducted to determine the atomic composition of the oxide. EDX shows the Tungsten, oxygen, and Indium, confirming the formation of WO3/ITO. Fig. 4 shows the FESEM images of surface morphology (Fig 4 (A)) and a cross-sectional view (Fig 4 (B)) of adding two %wt of NaDCC in WO3 thin film on ITO formed WO3@NaDCC /ITO. Comparing this with WO3 /ITO

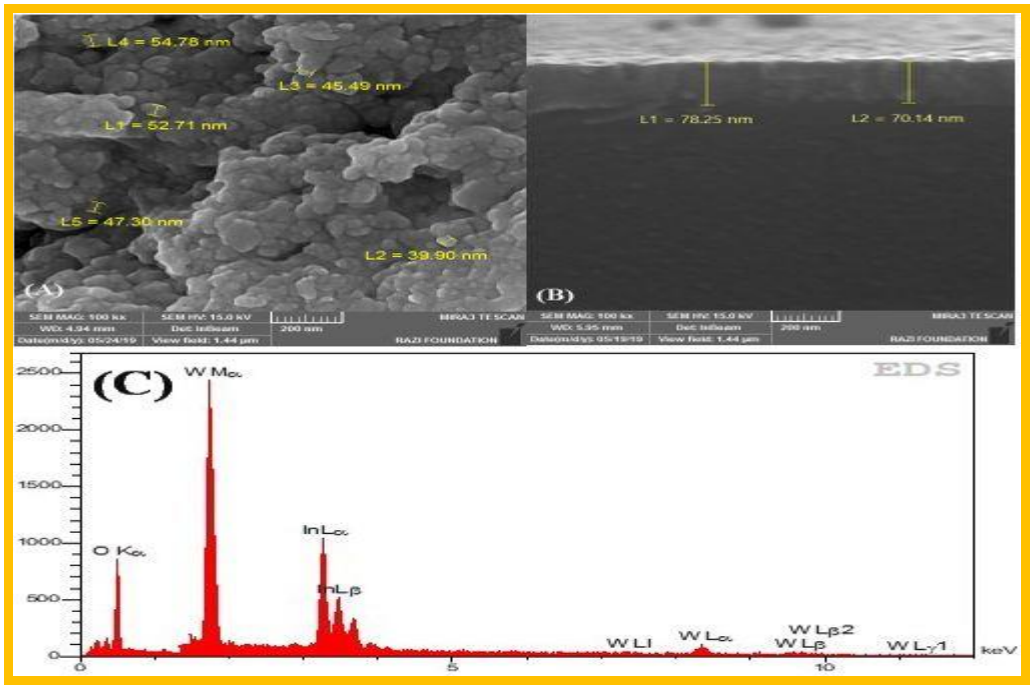

Figure3. FESEM images of pure nanoparticles WO3 thin films deposited on the ITO glass substrate, annealing T= 600^{O}C. (A) Surface morphology (inset: low magnification), (B) Cross-sectional view, and (C) EDS analysis of the nanoparticles WO3 /ITO.

Nanoparticles without adding NaDCC. The FESEM images of the formed oxide are cleaner and smoother. The diameter of the nanoparticles of WO3@ 2% wt NADCC on the ITO substrate is non-uniform with an average size of ~54 nm.

Although the WO3/ ITO diameter seen to increased as compared to aqueous derived samples, the thickness of the formed oxide rather thin; ~ 85 nm as observed from the cross-sectional view (Fig 4 (B)). In Fig 4 (C) is the EDX analysis of WO3@NaDCC/ITO thin film shows the oxygen, tungsten, and indium with some sodium content confirming the formation of WO3 /ITO and is somewhat similar as mentioned in the previous discussion for sample fabricated in WO3 /ITO without adding NaDCC (Fig 3(C)).

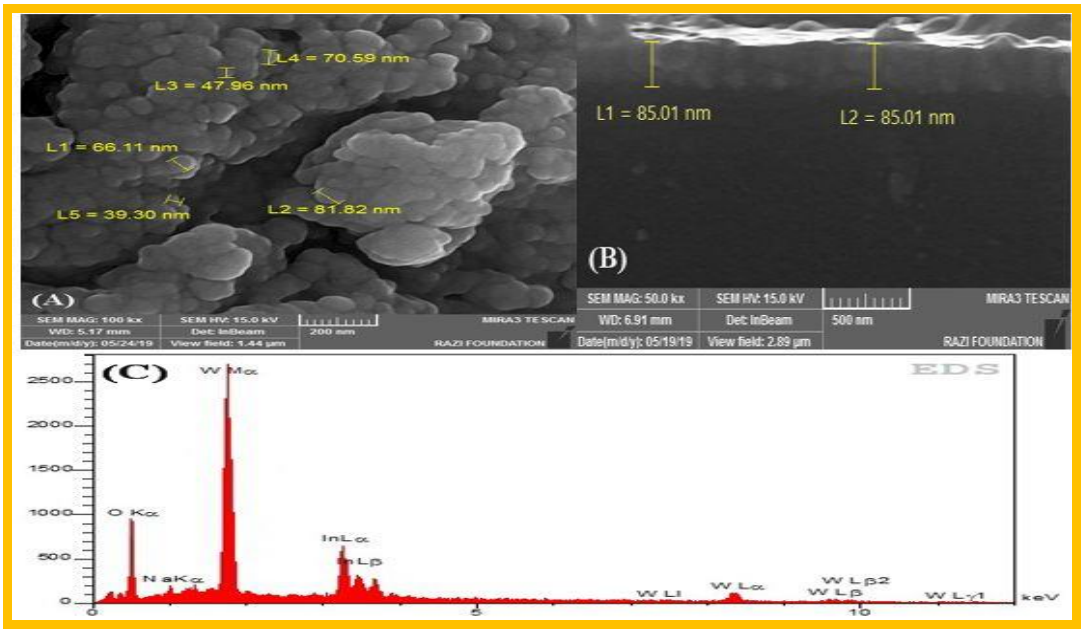

Figure4. FESEM images of WO3@(2)%NaDCC thin films deposited on the ITO glass substrate, for annealing T= 600^{O}C. (A) Surface morphology (inset: low magnification), (B) Cross-sectional view, and (C) EDS analysis of the nanoparticles WO3@, (2) %wt. / ITO.

When adding 4% of NaDCC in WO3/ITO thin film shows in Fig 5. The FESEM images of (A) surface morphology and the (B) cross-sectional view of the oxide subjected to annealing at 600 ^{o}C at all in the air.

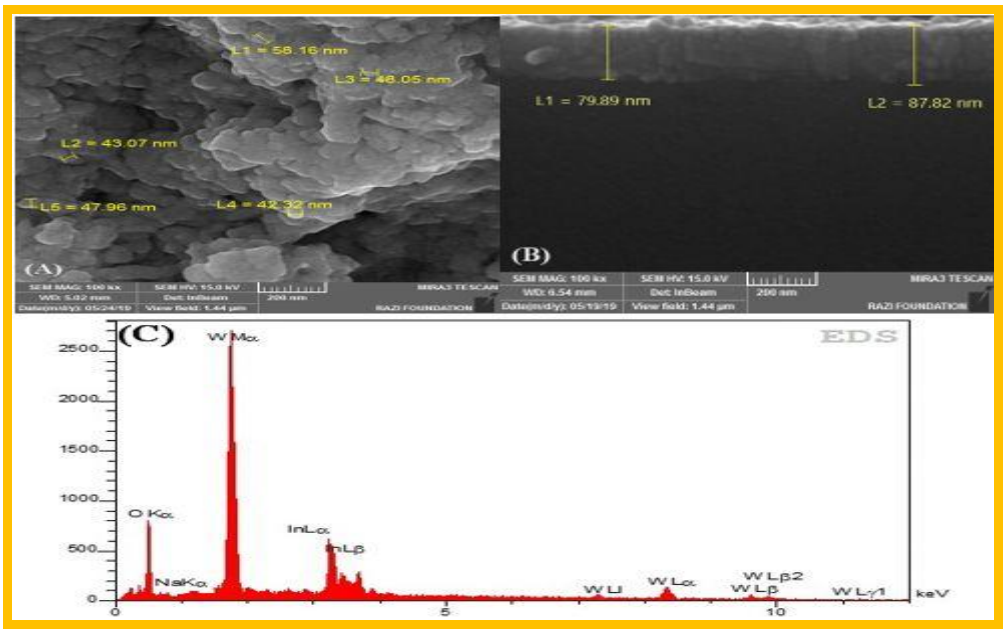

Figure5. FESEM images of WO3@(4)%NaDCC thin films deposited on the ITO glass substrate, for annealing T= 600^{O}C. (A) Surface morphology (inset: low magnification), (B) Cross-sectional view, and (C) EDS analysis of the nanoparticles WO3@, (4) %wt. / ITO.

The high temperature of thermal annealing for one h has as clearly shown in Fig 5 (A) from the top view. The average diameter of the WO3@ 4% NaDCC/ ITO thin film approximately ~82.5 nm. As shown in Fig 5 (B), Moreover, Fig 5(C) shows the EDX spectra of the WO3@4%NaDCC/ ITO that indicates the oxygen, tungsten, and indium but reduced in atomic size to confirm the formation of WO3/ITO thin films that underwent the annealing process at 600 ^{O}C. The thermal oxidation leads to the annihilation of the structure of the WO3 nanoparticles due to the excessive growth of the oxide. Consequently, the bottom part of the oxide (barrier layer) becomes thicker and form as compact oxide about 79.89 to 87.82 nm.

Electrical properties : Films were tested to confirm their semiconducting behavior. The film placed on a heater and their resistances is measured in the range from 30C˚ up to 200˚C, with a step of 10˚C, in the dry air atmosphere. The electrical resistivity of pure WO3 and doped NaDCC at different concentration films deposited on ITO glass was measured using the D.C. Two-point probe method. The conductivity follows the relation [16].

$$\sigma = \sigma_{\circ} \exp (- Ea / K_B T) \quad (7)$$

Where σ is resistivity at temperature T, $\sigma_{\circ}$ is a constant; K_B is Boltzmann constant ($1.38*10^{-23}$ j.sec), Ea is activation energy for conduction. By taking (Ln) of the two sides of equation (7), we can get :

$$Ln\ \sigma = Ln\ \sigma_{\circ} (- Ea / K_B T) \quad (8)$$

From the determination of the slope, we can find the activation energy:

$$Ea = K_B . \text{slope} \quad (9)$$

Fig 6 shows the variation of (Ln) of conductivity (Ln σ) with 1000/ T (K) $^{-1}$.For pure and doped NaDCC at different concentration films. Two stages of conductivity throughout the heating temperatures range noted, first activation energy (Ea1) occurs at low temperature, near Fermi level within the range (303-403) K. while the second activation energy (Ea2) K occurs at high temperatures within localized states at the range (403-473) K.

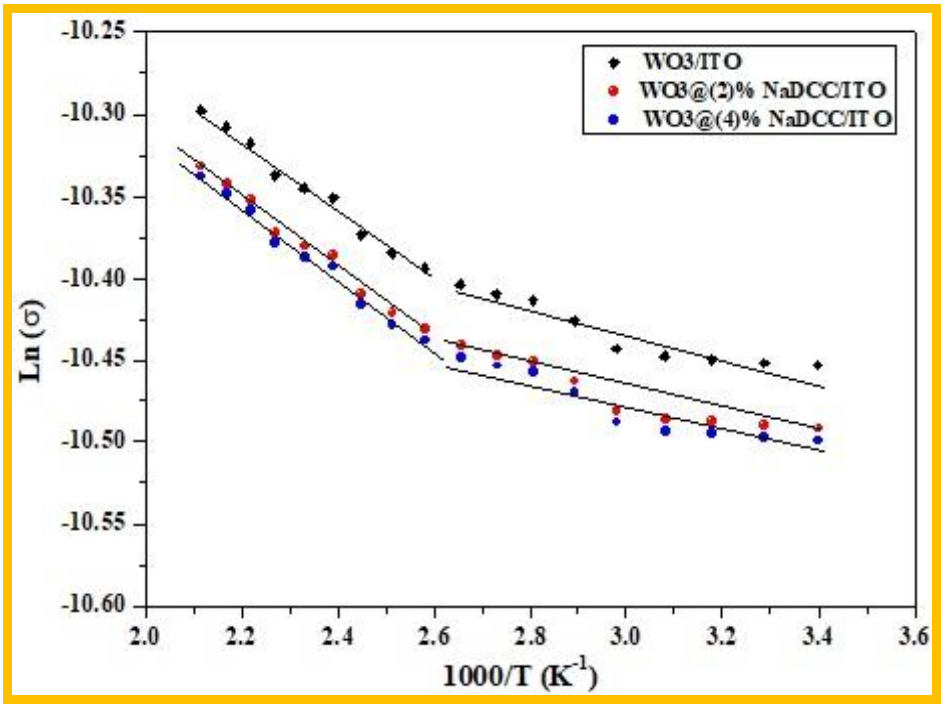

Figure 6. The graph shows the variation of (Lnσ) with (1000/T) for pure WO3 and doped NaDCC thin films at the different concentration on ITO glass substrate at temperature 600˚C.

The fig 6 shows that there is a decrease in conductivity with the increase in the doping, this is because, with the increase in annealing temperature, grain size increases resulting in a reduction of grain boundaries and associated impedance to the flow of charge carriers Such behavior is favorable for gas sensor applications of these films.

Table 5. D.C conductivity parameters for pure WO3 and doped NaDCC thin films at **the** different concentrations on ITO glass substrate at temperature 600˚C.

NaDCC %	E_{a1} (eV)	Temp. Range (K)	E_{a2} (eV)	Temp. Range (K)	σ_{RT} $(\Omega.cm)^{-1}$ x10^{-5}
0	0.0115	293-383	0.0108	383-473	2.89
2	0.0119	293-383	0.0112	393-473	2.78
4	0.0120	293-383	0.0113	393-473	2.76

The variation of carrier concentration (n_H) and Hall mobility (μ_H) of un-doped WO3 and doped with different concentration thin films of NaDCC on ITO glass after annealing at 600˚C shown in Fig. (7).

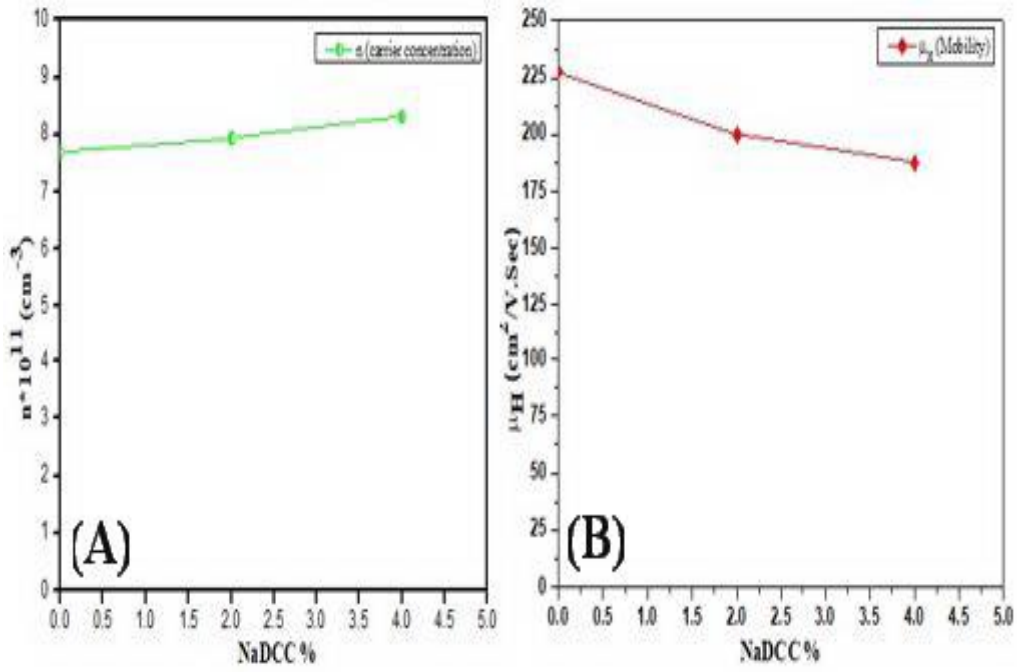

Figure 7. The graph shows (A) Variation of carrier concentration (n) with a dopant ratio of WO3@(0,2, and 4)%wt. NaDCC/ITO thin films at temperature 600˚C. (B) Variation of Mobility (u_H) with the dopant ratio of WO3@(0,2, and 4)%wt. NaDCC/ITO thin films at temperature 600˚C.

Hall measurements show that all those thin films have a negative Hall coefficient (n-type charge carriers). It attributed to the following two reasons [17].

1- The number of electrons is exciting above the conduction bands is larger than the number of holes is stimulating below the valance band.
2- The lifetime of free electrons is boosting from a negative defect state is higher than the lifetime of negative defect state free holes is exciting from a positive defect state.

Free holes excitation of positive defect state. It is clear from (see Tables 6) that the carrier concentration increases with dopant ratio while there were decreasing in carrier mobility (μH) with dopant concentration and the doping process was not affecting the type of the charge carriers. It leads to a decreasing in the disorder of the crystal lattice, which causes decreasing in phonon scattered and ionized impurity scattering and results in a decreasing in mobility.

Table 6. Hall parameters for pure WO3 and doped NaDCC thin films at **the** different concentration on ITO glass substrate at temperature 600˚C.

NaDCC %	σ_{RT} $(\Omega.cm)^{-1}$	μ_H $(cm^2/v.sec)$	R_H	n (cm^{-3}) *10^{13}	type
0	2.80467E-5	227.67369	8.12E+06	0.077	n
2	2.53718E-5	199.88648	7.88E+06	0.0793	n
4	2.49376E-5	187.46537	7.52E+06	0.0831	n

IV. CONCLUSION

The WO3 thin film with different doping concentration of NaDCC (0,2and 4) wt.% have been prepared on ITO glass substrate by hydrothermal technique at T =200˚C successfully. The diffraction pattern of WO3@NaDCC on ITO substrate with annealing temperature 600˚C revealed the structure would become polycrystalline for different doping concentration of NaDCC. The line broadening of undoped WO3 and doped WO3 with (2 and 4)%wt of NaDCC was due to small size of small crystallite size and lattice strain which were determined by D_{sh} formula , modified Williamson Hall was accepted to conclude the DW-H value and tension due to lattice deformation, spherical grains are observed to be about 45 nm . The FESEM study shows the agglomerated spherical nanoparticles. All prepared films have two activation energies Ea1 and Ea2 at range (303-473) K these activation energies decrease with the increasing of NaDCC concentration. Moreover, the D.C conductivity for all films at 600C˚ decreases with increase doped by NaDCC for all concentration.

REFERENCES

[1] S. A. A. Rizvi and A. M. Saleh, "Applications of nanoparticle systems in drug delivery technology," *Saudi Pharm. J.*, vol. 26, no. 1, pp. 64–70, 2018.

[2] F. T. M. Noori, A. Kadhim, and N. D. Hamza, "Optical and structural properties of ZnO: Au nanocomposite thin films," *Int. J. Nanoelectron. Mater.*, vol. 11, no. 3, pp. 347–356, 2018.

[3] R. O. Yathisha and Y. A. Nayaka, "Synthesis of copper oxide nanorods by microwave-assisted combustion route and their characterization studies," *Int. J. Nanoelectron. Mater.*, vol. 11, no. 2, pp. 233–240, 2018.

[4] A. Mirzaei, J.-H. Kim, H. W. Kim, and S. S. Kim, "Gasochromic WO_3 Nanostructures for the Detection of Hydrogen Gas: An Overview," *Appl. Sci.*, vol. 9, no. 9, p. 1775, 2019.

[5] S. Q. Yu, Y. H. Ling, R. G. Wang, J. Zhang, F. Qin, and Z. J. Zhang, "Constructing superhydrophobic WO_3@TiO_2 nanoflake surface beyond amorphous alloy against electrochemical corrosion on iron steel," *Appl. Surf. Sci.*, vol. 436, pp. 527–535, 2018.

[6] Y.-C. Liang and C.-W. Chang, "Preparation of Orthorhombic WO_3 Thin Films and Their Crystal Quality-Dependent Dye Photodegradation Ability," *Coatings*, vol. 9, no. 2, p. 90, 2019.

[7] T. Soltani, A. Tayyebi, H. Hong, M. H. Mirfasih, and B. K. Lee, "A novel growth control of nanoplates WO_3 photoanodes with dual oxygen and tungsten vacancies for efficient photoelectrochemical water splitting performance," *Sol. Energy Mater. Sol. Cells*, vol. 191, no. May 2018, pp. 39–49, 2019.

[8] W. Zhao, X. Wang, L. Ma, X. Wang, W. Wu, and Z. Yang, "WO $_3$p-Type-GR Layered Materials for Promoted Photocatalytic Antibiotic Degradation and Device for Mechanism Insight," *Nanoscale Res. Lett.*, vol. 14, pp. 1–10, 2019.

[9] A. L. Santhosha, S. K. Das, and A. J. Bhattacharyya, "Tungsten Trioxide (WO_3) Nanoparticles as a New Anode Material for Sodium-Ion Batteries," *J. Nanosci. Nanotechnol.*, vol. 16, no. 4, pp. 4131–4135, 2016.

[10] M. M. Momeni, Y. Ghayeb, and F. Ezati, "Fabrication, characterization and photoelectrochemical activity of tungsten-copper co-sensitized TiO_2 nanotube composite photoanodes," *J. Colloid Interface Sci.*, vol. 514, pp. 70–82, 2018.

[11] M. B. Tahir, M. Sagir, and K. Shahzad, "Removal of acetylsalicylate and methyl-theobromine from the aqueous environment using nano-photocatalyst WO_3-TiO_2 @g-C3N4 composite," *J. Hazard. Mater.*, vol. 363, pp. 205–213, 2019.

[12] S. Park, "Enhancement of hydrogen sensing response of ZnO nanowires for the decoration of WO_3 nanoparticles," *Mater. Lett.*, vol. 234, no. September, pp. 315–318, 2019.

[13] W. H. Organization, "N-Nitrosodimethylamine in drinking-water. Background document for development of WHO Guidelines for Drinking-water Quality," *WHO, Geneva, Switz.*, pp. 1–36, 2008.

[14] S. Dichloroisocyanurate and C. Dioxide, "in Laboratory Waters of Varying Turbidity," 2019.

[15] J. Ram, R. G. Singh, R. Gupta, V. Kumar, F. Singh, and R. Kumar, "Effect of Annealing on the Surfaces Morphology, Optical and Structural Properties of Nanodimensional Tungsten Oxide Prepared by Coprecipitation Technique," *J. Electron. Mater.*, vol. 48, no. 2, pp. 1174–1183, 2019.

[16] R. Rathika *et al.*, "Effect of 200 MeV Ag $^{15+}$ ion beam irradiation at different fluences on WO_3 thin films," *Nucl. Instruments Methods Phys. Res. Sect. B Beam Interact. With Mater. Atoms*, vol. 439, no. June 2018, pp. 51–58, 2019.

[17] Z. N. Jameel, O. A. Mahmood, and F. L. Ahmed, "Studying the Effect of Synthesized Nano-Titanium Dioxide via Two Phases on the Pseudomonas Aeruginosa and Portus Bacteria as Antimicrobial Agents," vol. 12, no. 3, pp. 329–338, 2019.